UCRL-JRNL-228617

LAWRENCE
LIVERMORE
NATIONAL
LABORATORY

Quantitative electron and gas cloud experiments

A. W. Molvik, M. Kireeff Covo, R. H. Cohen, A. Friedman, W. M. Sharp, D. Baca, F. M. Bieniosek, C. Leister, P. A. Seidl, J.-L. Vay

March 4, 2007

Nuclear Instruments and Methods A

Disclaimer

This document was prepared as an account of work sponsored by an agency of the United States Government. Neither the United States Government nor the University of California nor any of their employees, makes any warranty, express or implied, or assumes any legal liability or responsibility for the accuracy, completeness, or usefulness of any information, apparatus, product, or process disclosed, or represents that its use would not infringe privately owned rights. Reference herein to any specific commercial product, process, or service by trade name, trademark, manufacturer, or otherwise, does not necessarily constitute or imply its endorsement, recommendation, or favoring by the United States Government or the University of California. The views and opinions of authors expressed herein do not necessarily state or reflect those of the United States Government or the University of California, and shall not be used for advertising or product endorsement purposes.

Quantitative electron and gas cloud experiments*

A.W. Molvik, M. Kireeff Covo, R. H. Cohen, A. Friedman, W. M. Sharp, Lawrence Livermore National Laboratory, Livermore, CA 94550 USA; David Baca, F. M. Bieniosek, C. Leister, P. A. Seidl, J-L. Vay, Lawrence Berkeley National Laboratory, Berkeley, CA 94720-8139

Abstract

Electrons can accumulate in and degrade the quality of positively charged beams. This is a well-known problem in proton storage rings. Heavy-ion rings are more frequently limited by gas pressure-rise effects. Both effects may limit how closely the beam radius can approach the beam-tube radius in a heavy-ion linac. We study beams of 1 MeV K^+ with currents of up to 180 mA in the High-Current Experiment (HCX), and compare our work with simulations. The theory simulation results are discussed in a companion papers. We have developed the first diagnostics that quantitatively measure the accumulation of electrons in a beam [3]. This will enable the particle balance to be measured for each source of electrons in a linac: ionization of gas, emission from walls surrounding the beam, and emission from an end wall coupled with electron drifts upstream through quadrupole magnets, and electron-trapping efficiencies can be determined. Experiments where the heavy-ion beam is transported with solenoid magnetic fields, rather than with quadrupole magnetic or electrostatic fields, are being initiated. We discuss plans for experiments using electrode sets (in the middle and at the ends of magnets) to either expel or to trap electrons within the magnets. We observe oscillations of the electron density and position in the last quadrupole magnet when we flood the beam with electrons from an end wall. These oscillations, near 6 MHz, are observed to grow from the center of the magnet while drifting upstream against the beam, in good agreement with simulations.

PACS: 29.27.Bd, 41.75.Ak, 52.25.Wz, 52.70.Nc

Keywords: electron cloud, quadrupole, solenoid, retarding-field analyzer, clearing, diagnostics

Corresponding author: Arthur W. Molvik, molvik1@llnl.gov, L-637, LLNL, Livermore CA 94550, USA. Phone (510) 846-6613, Fax (510)846-5392

Introduction

Electron clouds and gas pressure rise limit the performance of many major accelerator rings, and may limit linacs being developed as drivers for heavy-ion-inertial fusion (HIF) [1] and for warm-dense matter physics (WDM) [2]. Linacs for HIF and WDM are at risk because the cost of the accelerators increases for larger beam tubes, therefore we need to shrink beam tubes as tightly to the beam as possible, causing beam-halo to scrape the beam tubes. This will result in increased electron or gas emission until these become large enough to reduce the beam quality, restricting further reductions in beam-tube radius. We are working to understand the underlying physics through the coordinated application of experiment, theory, and simulation. This paper emphasizes the experimental component, accompanying papers discuss theory and simulations [3,4].

Electron cloud effects generally occur gradually, over many passes of a beam through an accelerator ring. However, we have demonstrated in both experiment and simulation that high electron densities, approaching the beam density, can significantly degrade beam properties in the short distance of 2 lattice periods in a linac.

We study these effects in the High-Current Experiment (HCX), shown in Fig. 1. HCX transports a 4 μs flattop pulse (superbunch-like) of 0.18 A of 1 MeV K+ ions. Details of the beam transport through 10 electrostatic quadrupoles, preceding the 4 magnetic quadrupoles, have been reported [5]. The beam has a space-charge potential of 2 kV, corresponding to a tune depression to 0.10 in a long lattice. This potential approaches that of high-energy physics (HEP) and other accelerator rings and is sufficient for many experiments on the generation, accumulation, effects, and mitigation of electron-cloud effects.

1. Diagnostics and electron control electrodes

The HCX, in the region of four magnetic quadrupoles, is shown in Fig. 1. To the left is the D2 diagnostic region between 10 electrostatic quadrupoles and the 4 magnetic quadrupoles. The D2 drift region contains diagnostics to characterize the beam entering the magnetic quadrupoles. A diagnostics tank, D-end, following the magnetic quadrupoles contains diagnostics to characterize the beam there, and determine whether the beam has changed since D2, in particular if it has been degraded through interaction with electron or gas clouds.

Each magnetic quadrupole has 30 cm long magnetic field coils in a 47 cm length elliptical tube that has major and minor inner radii of 5 cm and 3 cm respectively. Between each pair of magnets, and after the last one, diagnostic access is provided through 7 ports to a 5 cm axial gap. Arrays of diagnostics are mounted on the outside of 34 cm long octagonal tubes that fit within the elliptical-quadrupole-magnet beam tubes. Two different arrays are placed within the third and fourth quadrupoles. A gap of about 0.7 cm annular space is provided between the octagonal diagnostics mounting tube and the elliptical magnet bore for the recessed diagnostics and cables. These diagnostics include electrodes shielded from the beam electric field by grids that we will discuss further here, recessed capacitive electrodes, and nearly square 8 cm^2 electrodes that are flush with the diagnostics tube in the fourth quadrupole.

The radial gradient of the quadrupole magnetic field is approximately 10 T/m in each of the magnets. This provides magnetic fields of up to 0.3 to 0.5 T at the beam tubes. This

is sufficient to strongly magnetize electrons, although cold ions from beam-impact ionization of gas are not magnetized and are expelled across the magnetic field. The current of expelled cold ions can be measured to determine the gas pressure within the beam [6]. Electrons, at low densities, drift through the magnets at a velocity of 0.6 m/μs, compared with the beam velocity of 2.2 m/μs.

A suppressor ring electrode, surrounding the beam after it exits the last quadrupole magnet, is biased to –10 kV to prevent ion-induced electron emission off an end wall (a slit plate) from reaching the magnets, or it can be left unbiased to allow electrons to be emitted from the end wall and to flow upstream into the magnets. In recent experiments, we replaced the ring electrode with a pair of parallel plates – both of these can be biased negatively to suppress electron emission similar to the ring suppressor; but they can also be biased to produce an electric dipole field across the beam. Electrons are then attracted to the positive plate, enabling electron emission from the end wall plus ionization of desorbed gas to be measured.

When the suppressor electrode(s) are biased negatively, they also prevent electrons from leaving the beam at the exit of the four quadrupole magnets. At the entrance to the magnetic quadrupoles, the exit electrode of the electrostatic quadrupoles is also negative, which prevents electrons from being lost upstream of the quadrupole magnets. These electrodes provide axial confinement and the positive-ion beam potential provides radial confinement of electrons, so that electrons are confined both axially and radially. Once trapped, we expect electrons to remain trapped until the beam potential decreases at the end of the pulse, unless removed earlier by clearing electrodes, or induction acceleration gaps.

New quantitative measurements

We briefly review diagnostics that we have developed to provide quantitative measurements of electron clouds, and which can be used to verify simulations.

We are using a retarding field analyzer (RFA), which incorporates our previous experience [7]. It uses the simplified construction of the Rosenberg-Harkay design [8], but with the addition of a grid that serves as an ion repeller, Fig. 2 [9]. Other investigators have used similar analyzers to measure the flux and energy of electrons reaching the wall, yielding a qualitative measurement of electron cloud density. We measure the expelled ion energy distribution, which perhaps counter-intuitively provides a more quantitative measurement of electron cloud density than does measuring electrons directly. This is because we measure low energy ions resulting from beam impact on gas, which are expelled by the beam potential, providing a measurement of the potential and of the degree to which it is reduced by the accumulation of electrons [9].

Electron currents to clearing electrodes provide an independent and corroborating measurement of electron accumulation as a function of time. When they are biased positively, they remove electrons that would otherwise accumulate between the negative electrodes at either end of the quadrupole magnets. Integration of this current yields the time-dependent electron line charge that would accumulate in the case when clearing electrodes are off.

To obtain the line charge of electrons when clearing electrodes are on, we divide the clearing electrode current by the electron drift velocity in quadrupole magnets. This has been determined in simulations [10] and in experiments to be about 0.6 m/μs.

We studied the scaling of electron emission with K+ ion energy between 50 and 393 keV. due to ions impinging at angles near grazing incidence on stainless steel. This information is needed to provide the electron source term resulting from halo scraping, as well as to calibrate diagnostics to determine halo loss from measurements of electron emission. We found that emission scaled with the electronic component of ion stopping in stainless steel, dE/dx [11], as has been found previously at higher energies [12]. However, the emission did not vary with 1/cos(θ), unlike measurements with 1 MeV K+ [13] and higher energy heavy ions [14]. We have successfully modeled angle of incidence variation, with a modified dE/dx model [11].

Simulations by the WARP/POSINST PIC code show oscillations in electron density and position that grow and propagate upstream against the beam when we intentionally flood the beam with electrons by turning off the electron suppressor electrode(s). The simplest experimental diagnostic of this is the current to a clearing electrode. The clearing electrode can also be simulated, the results are shown in Fig. 3. Good agreement is obtained for both the frequency and amplitude of oscillations. Work is continuing to experimentally test other predictions of simulations, to identify the causes of the oscillations, and to determine whether this effect is an instability.

Emerging measurements of trapped electrons

We have established the quantitative validity of some of the electron and gas diagnostics that we are using, as discussed in the preceding section as well as at the preceding HIF Symposium [6]. Other diagnostics have not been validated to the same degree, but are providing additional unique information that has, at least, qualitative validity.

One method of measuring the accumulation of electrons at the end of a beam pulse would be to measure the current of electrons that detrap during the beam tail when the beam potential is falling to zero. To accomplish this, it is important to shield the capacitively-coupled current from the beam head and tail; because the magnitude and polarity of the integrated charge at the end of a pulse for a capacitively coupled beam with no electrons is the same as the electron charge collected from a completely neutralized beam. Furthermore, if electrons only partially neutralize the ion beam, their charge will be much smaller than the capacitively coupled charge at the beam tail. In addition to shielding against capacitive pickup, if the collectors are in a magnetic field, it is essential that the collectors be located where electrons can flow along field lines to the collector from electron cloud locations in the beam and its vicinity.

To satisfy these conditions, gridded-electron collectors (GEC) are located at azimuths where quadrupole field lines enter the beam tube, see Fig. 4. Then, electrons that are detrapped as the beam potential falls to zero at the end of the pulse can flow along magnetic field lines from the beam to the collector. Preliminary results were discussed at PAC05 [15]. This azimuthal location forgoes the magnetic suppression that is achieved with gridded ion collectors (GIC) by locating them at azimuths where magnetic field lines are tangent to the surface [14], but which would also render collection of

magnetized electrons impossible. A consequence of this location is that we can bias the collector to suppress electron emission from either the collector or the grids, but not from both.

As mentioned, the purpose of the grids is to shield the GIC/GEC from capacitive pickup, which exceeds the expected current of expelled ions or detrapped electrons by 3 orders of magnitude. The effectiveness of the grids was tested before installation by pulsing square waves on a metal cylinder at the beam position, relative to the grounded diagnostics beam tube. The signal to gridded collectors was compared with the signal to bare collectors, scaled to the same area, to determine the shielding factor of the grids. Electromesh grids of 90 mesh/inch, 90% transparency, were sandwiched between the stainless steel diagnostics beam tube and a thin stainless steel frame, which was spot-welded around the periphery, grounding the grids to the diagnostics beam tube. A single grid provided a shielding factor of 30, which was inadequate compared with the expected capacitive pickup. Adding a second grid, with one on the inside and one on the outside of the 0.4 mm thick beam tube, increased the shielding factor to an adequate 400-600.

During commissioning tests [15], we found that the GEC current-voltage characteristic was flat within 10% for positive collector bias between 20 and 80 V. This satisfies one requirement for reliable GEC measurements: the current doesn't vary significantly with the collector bias. Then, setting the bias is not critical, and we do not need to justify why one particular bias produces the correct current, when other values for the bias would produce different currents.

The effects of the collector bias are compared for positive and negative bias in Fig. 5. During most of the pulse the polarity of the current reverses from collecting electrons on

a positive electrode to emitting electrons from a negative electrode; however at two times in the beam tail, the current to a negatively biased electrode becomes negative (see the next paragraph). In Fig. 5, we also compare the current to the Faraday cup located after the magnets, which we correct for time-of-flight to shift to the GEC axial position. We use capacitive pickup from the beam to the flush short collectors (FLS) at the same axial position as the GEC to align the beam head, determining the time-shift.

We plot the GEC current as a function of the electron trapping energy in Fig. 6. We obtain the trapping energy from the Faraday cup current decay at the end of the pulse as follows: The peak beam potential on axis with minimal electrons is 2000 V [9,16]. We set the point where the beam current begins a more rapid decay to zero (~9.5 μs), and the end of the current decay to 2000 V (~10.5 μs), scaling potentials in between to be proportional to the change in beam current. When we compare both polarities of GEC collector bias, we see certain periods that despite a negative bias, which repels low energy electrons, still have a negative current: we believe that at those periods, extreme scrape off of beam halo generates an electron cloud that is dense enough to overcome the negative electrode bias to yield an electron current into the collector. At other times, emission from the electrode gives a positive current. The periods with negative current to a negatively-biased electrode correspond to ~600 V and 1100 V trapping potential so we regard the GEC currents as suspect near these times.

To obtain the electron line charge, we observe that the GEC's not only collect electrons from all magnetic flux that passes through the beam but also from most of the remaining region outside the beam. Since quadrupole fields have four similar regions azimuthally, we multiply the measured signal to one of these regions by 4. Axially, the

GEC aperture is 2.8 cm long, and the transmission of the double grid totals 0.77, so we can obtain the line-charge per meter from the integrated electron charge to the GEC collector during the beam tail by multiplying by (4/(0.028*0.77)) = 186. Applying this factor and numerically integrating the negative tail spike, we obtain the electron line-charge λ_e, which can be normalized to the ion beam charge (λ_b = 0.082 μC/m), yielding $\lambda_e/\lambda_b \approx 0.14$. This compares with $\lambda_e/\lambda_b \approx 0.07$ two magnets upstream, determined from clearing electrode currents and electron drift velocities [9].

We check our interpretation of the weakly and deeply trapped electrons measured by the GEC by varying the clearing-electrode bias: we find that the peak that we label as weakly-trapped electrons is removed by a clearing bias of only 150-300 V, whereas removal of the peaks that we label as deeply-trapped electrons requires ≥1000 V, see Fig. 7. This is just the behavior that we would expect for accumulated electrons: weakly trapped electrons have turning points at larger radii, so require relatively low clearing bias to shift the turning points into the clearing electrodes. Deeply trapped electrons, on the other hand, have turning points at smaller radii, which are further from the clearing electrodes, so require higher clearing bias to shift these electrons out to the clearing electrodes. If the GEC were only measuring electrons as they were produced, then both the peaks that we label as weakly and deeply trapped would consist of electron just produced at a beam tube, and both peaks would be removed with the same ease by the clearing electrodes.

To recapitulate, the final peak of the GEC current, corresponding to deeply-trapped electrons, is difficult to interpret in a quantitative manner: Beam scrape off of the tail contributes to a portion of the current measured during the detrapping of these electrons.

Secondary electron emission from the grids, the opposite wall along magnetic field lines, and the collector cannot all be suppressed by biasing the collector. So measurements of deeply-trapped electrons are only qualitative at present. Quantitative measurements of weakly-trapped electrons to within about a factor of 2 appear to be currently achievable, based on comparison with RFA beam-potential measurements. The direction of the factor depends on the polarity of the GEC collector bias.

The analysis presented here presupposes that electrons are electrostatically trapped, not magnetically trapped. This seems reasonable: with our long 5 μs duration beam pulse we do not have the multipactoring resonance with the electron bounce time that is present in radio-frequency (rf) accelerators, so for an electron line charge of much less than that of the beam, electrons from either the wall or ionization of gas should not become magnetically trapped. However, we have evidence that these arguments are not valid during electron density oscillations, because the simulations show that electrons actually reverse the +2 kV beam potential to approximately –1 kV, which we believe is possible only with magnetized electrons. A second exception is that calculations by R. H. Cohen show that in the region near the axis with near zero magnetic field, the electron magnetic moment is no longer conserved but can change in jumps, electrons could be magnetically trapped for up to a few hundred bounces ($\leq$1 μs). A third exception would be if rf waves in the vicinity of the electron cyclotron frequency ($\leq$5 Ghz) were present, electrons could gain energy and would become magnetically trapped for sufficiently high amplitude rf.

In future work, we plan to study weakly-trapped electrons, that in Fig. 6 appear to have a trapping width of ~400 eV. If these electrons originate from the beam tube, we would expect a narrower trapping width. We will examine possible causes for this,

including relaxing the assumptions discussed above. This will complement other studies that capitalize on our new capabilities to measure absolute electron line charge as a function of time in order to measure electron accumulations from different sources, and to determine the sensitivity of the beam to varying amounts of electrons from each source.

Plans for electron experiments in solenoids

We have been studying electron clouds in quadrupole magnets, which have been used for ion beam transport at high energies in most HIF driver concepts. However, solenoids have potential advantages in transporting higher line charge densities than quadrupoles, especially at low energies, and have also been demonstrated to suppress electron clouds when applied to drift regions of positron rings [17]. We are therefore initiating a study of heavy-ion transport in solenoids, in the Solenoid Transport Experiment (STX), which will include electron and gas cloud studies [18]. Our overall strategy in comparing solenoid and magnetic quadrupole transport is to simulate each, verifying the code predictions with experiment where feasible.

Our initial experiments will use analogs of the clearing electrodes that have provided reduction of electron clouds and their effects, and have also provided quantitative measurements of electron densities [9]. We are installing a series of biased rings, Fig. 8, that are intended to provide a choice of removing electrons or confining them. The short rings are installed in the center of a solenoid magnet, the longer rings in the expanding magnetic flux between magnets. For initial experiments, the magnetic field direction will be the same through the four solenoids.

The rings within solenoid magnets are short, so that an axial electric field exists throughout the magnet to expel electrons when biased negatively, see Fig. 9. This avoids a population of low-energy electrons that drift slowly through the ring, which could happen with a long ring where the axial electric field was zero except near the ends.

The rings between solenoids are longer, to intercept as much as possible of the magnetic flux that expands between magnets. This enables these electrodes to suppress electrons closer to the beam axis: for one possible envelope, to the outer 8% of the beam radius in the first magnet nearest the injector, and to the outer ~50% of the beam radius in the last two magnets.

We can choose to expel or confine electrons on field lines intercepting the long-electrode. To expel electrons, we bias the short electrodes within the magnet negatively to repel electrons and the long electrodes positively to attract electrons and suppress electron emission, using bias potentials of up to 2-3 times the beam potential. To confine electrons, we reverse these potentials, which will encourage electron emission from the long electrodes, and attract them to the short electrodes; this is effectively a Penning Trap geometry, with radial confinement by magnetic fields and axial confinement by electric fields. This generates an axial electric field that reverses direction at every electrode. Either polarity can trap electrons on inner flux surfaces that do not intercept the long electrodes.

Electrons on inner flux surfaces can originate from ionization of gas, or from structures at the end that generate electrons, which flow into the magnets along magnetic field lines. In principle, these electrons can also be expelled or trapped by biasing the electrode array to generate a uni-directional electric field along the beam axis that drives

electrons towards or away from the end wall, respectively. With an electric field of 400 V/m, electrons can be expelled to the far end in 250 ns. Shielding of these potentials by the high-space charge beam can be evaluated with simulations.

We can also investigate solenoid transport where the magnetic field reverses direction in adjacent magnets or groups of magnets. At each reversal, all the magnetic flux intercepts the long electrodes, providing a tool to suppress or to increase electrons throughout the beam cross sectional area.

In summary, we have developed absolute measurements of electron-cloud density with a retarding field analyzer and clearing electrodes. Our simulations of electron oscillations within quadrupole magnets agree quantitatively with clearing-electrode measurements. We are able to distinguish weakly-trapped from deeply trapped electrons within quadrupole magnets by measuring their detrapping at the end of a pulse. Finally we described plans to diagnose and to reduce or to increase electrons in a solenoid, to begin comparing of these with electrons in quadrupole magnets.

*Experimental operations were ably supported by Wayne Greenway, Takeshi Katayanagi, Craig Rogers, and Edgardo Romero II. This work performed under the auspices of the U.S Department of Energy by University of California, Lawrence Livermore and Lawrence Berkeley National Laboratories under contracts No. W-7405-Eng-48 and DE-AC02-05CH11231.

References

[1] B. G. Logan, F. M. Bieniosek, C. M. Celata, et al., "Overview of the US heavy ion fusion research," Nuclear Fusion 45 (2005) 131.

[2] J. J. Barnard, et al., this conference.

[3] R. H. Cohen, et al., this conference.

[4] J-L. Vay, et al., this Conference

[5] L. R. Prost, P. A. Seidl, F. M. Bieniosek, C. M. Celata, A. Faltens, D. Baca, E. Henestroza, J. W. Kwan, M. Leitner, W. L. Waldron, R. Cohen, A. Friedman, D. Grote, S. M. Lund, A. W. Molvik, and E. Morse, "High current transport experiment for heavy ion inertial fusion," Phys. Rev. Special Topics – Accelerators and Beams (PRSTAB) 8 (2005) 020101.

[6] A.W. Molvik, P. A. Seidl, F. M. Bieniosek, R. H. Cohen, M. Kireeff Covo, L. Prost, "Experimental Studies of Electrons in a Heavy-Ion Beam", Nuc. Instrum. and Methods A, 544 (2005) 194.

[7] Arthur W. Molvik, "Large acceptance angle retarding-potential analyzers," Rev. Sci. Instrum. 52 (1981) 704.

[8] R. A. Rosenberg, and K. Harkay, Nucl. Instrum. Methods A 453 (2000) 507.

[9] M. Kireeff Covo, Arthur Molvik, Alex Friedman, Jean-Luc Vay, Peter Seidl, Grant Logan, David Baca, and Jasmina L. Vujic, "Absolute Measurement of electron cloud density in a positively-charged particle beam," Phys. Rev. Lett. 97 (2006) 054801.

[10] R. H. Cohen, A. Friedman, S. Lund, A. W. Molvik, ,E. P. Lee, T. Azevedo, J.-L. Vay, P. Stoltz, and S. Veitzer, "Electron-Cloud Simulation and Theory for High-Current Heavy-Ion Beams," Phys. Rev. Special Topics – Accelerators and Beams 7 (2004) 124201.

[11] M. Kireeff Covo, Arthur Molvik, Alex Friedman, Glen Westenskow, John J. Barnard, Ronald Cohen, David Grote, and Steven M. Lund, Peter Seidl, Joe W. Kwan, Grant Logan, David Baca, Frank Bieniosek, Christine M. Celata, and Jean-Luc Vay, Jasmina L. Vujic, "Beam Energy Scaling of Ion- Induced Electron Yield from K^+ Impact on Stainless Steel," PRSTAB 9 (2006) 063201.

[12] H. Rothard, K. Kroneberger, A. Clouvas, E. Veje, P. Lorenzen, N. Keller, J. Kemmler, W. Meckbach and K.–O. Groeneveld, Phys. Rev. A 41 (1990) 2521.

[13] A. W. Molvik, et al., "Gas desorption and electron emission from 1 MeV potassium ion bombardment of stainless steel," PRSTAB 7 (2004) 093202.

[14] P. Thieberger, et al., Phys. Rev. A61 (2000) 042901.

[15] A.W. Molvik, M. Kireeff Covo, A. Friedman, R. Cohen, S.M. Lund, J.J. Barnard, LLNL; F. Bieniosek, P. Seidl, D. Baca, J.-L. Vay, C.M. Celata, W.L. Waldron, LBNL; J.L. Vujic, UC Berkeley, "Experiments Studying Desorbed Gas and Electron Clouds in Ion Accelerators," 2005 Particle Accelerator Conference, Knoxville, TN, May 16-20, 2005.

[16] S. Lund, private communication (2004).

[17] A. Kulikov, A. Novokhatski, and J. Seeman, Proceedings of E-Cloud04; available at http://mafurman.lbl.gov/ECLOUD04_proceedings/kulikov_ECInst-v2.pdf

[18] P. A. Seidl, proceedings of this conference.

Figure Captions

Figure 1. HCX in region of 4 quadrupole magnets, with clearing electrode rings between magnets and a suppressor electrode ring after the last magnet.

Figure 2. Retarding field analyzer (RFA) includes ion repeller grid to enable ion as well as electron energy distribution measurements.

Figure 3. Current to clearing-electrode ring preceding final quadrupole magnet, when beam flooded with electrons by turning off suppressor electrode. Measured and simulated currents are compared.

Figure 4. Gridded electron collector (GEC) is located azimuthally in quadrupole magnet so that electrons, which detrap, can reach collector along magnetic field lines.

Figure 5. The currents to a gridded electron collector (GEC) are shown for negative and positive collector bias, and are compared to the time dependence of the end Faraday cup, which is time shifted to the GEC axial position. The suppressor is biased to V_s = -10 kV, and the three clearing electrodes are all biased to +9 kV.

Figure 6. Current of detrapped electrons at end of pulse as a function of trapping potential. Data from 8 Nov. 2004.

Figure 7. Weakly-trapped electrons (GEC first peak at end of pulse) are removed with lower clearing electrode bias than are deeply-trapped electrons (GEC final peak at end of pulse). Data from 23 June 2005.

Figure 8. Biased rings at center and between solenoid magnets are designed to expel or to trap electrons on outer flux lines that intercept the rings between magnets.

Figure 9. Equipotential contours from biasing a long ring between solenoids and short rings at center of solenoid magnets.

Figures & Captions: Molvik_HIF06

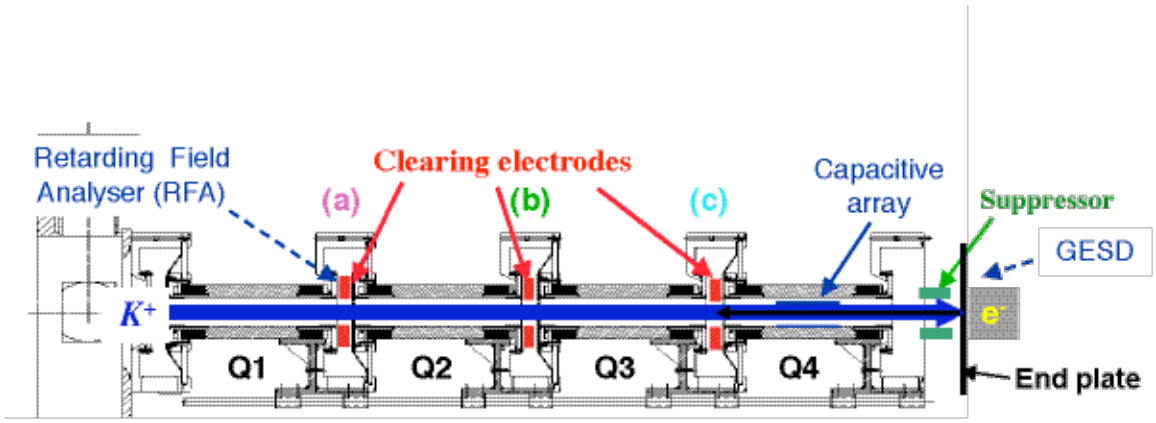

Figure 1. HCX in region of 4 quadrupole magnets, with clearing electrode rings between magnets and a suppressor electrode ring after the last magnet.

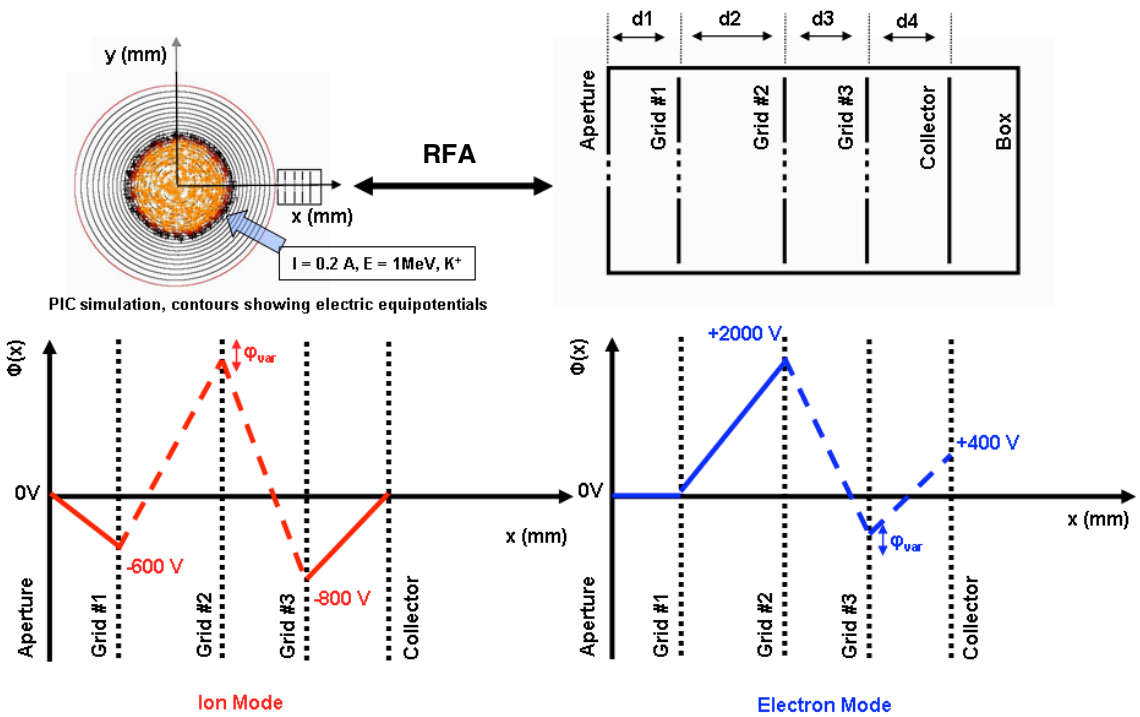

Figure 2. Retarding field analyzer (RFA) includes ion repeller grid to enable ion as well as electron energy distribution measurements.

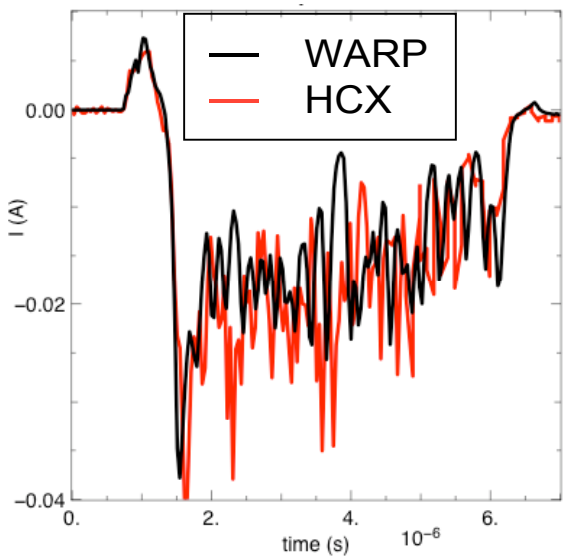

Figure 3. Current to clearing-electrode ring preceding final quadrupole magnet, when beam flooded with electrons by turning off suppressor electrode.

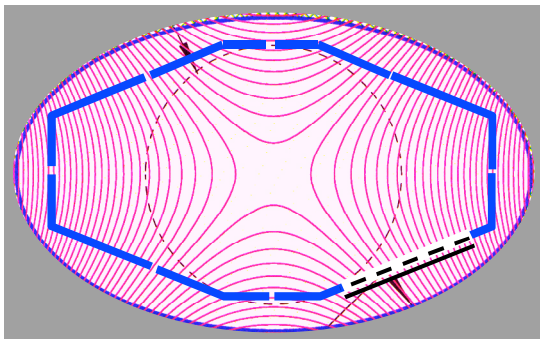

Figure 4. Gridded electron collector (GEC) is located azimuthally in quadrupole magnet so that electrons, which detrap, can reach collector along magnetic field lines.

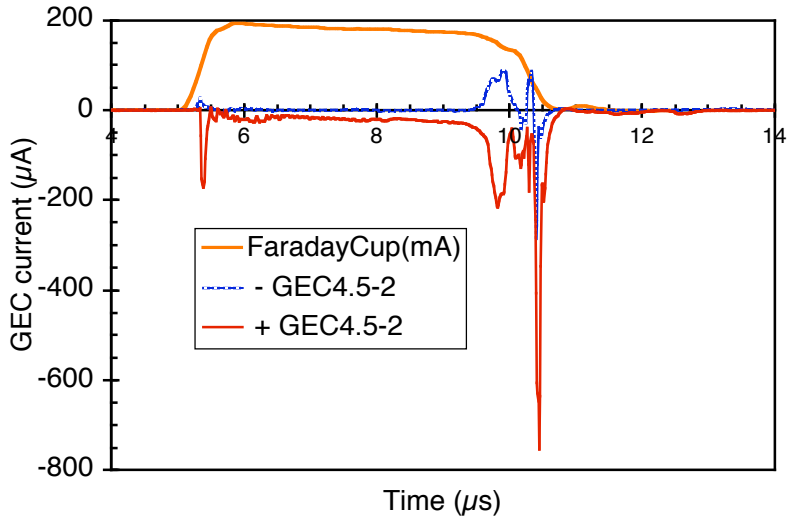

Figure 5. The currents to a gridded electron collector (GEC) are shown for negative and positive collector bias, and are compared to the time dependence of the end Faraday cup, which is time shifted to the GEC axial position. The suppressor is biased to V_s = -10 kV, and the three clearing electrodes are all biased to +9 kV.

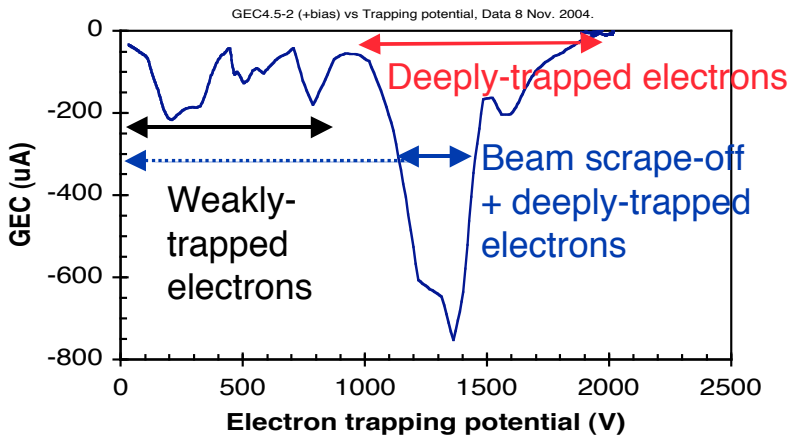

Figure 6. Current of detrapped electrons at end of pulse as a function of trapping potential, see text.

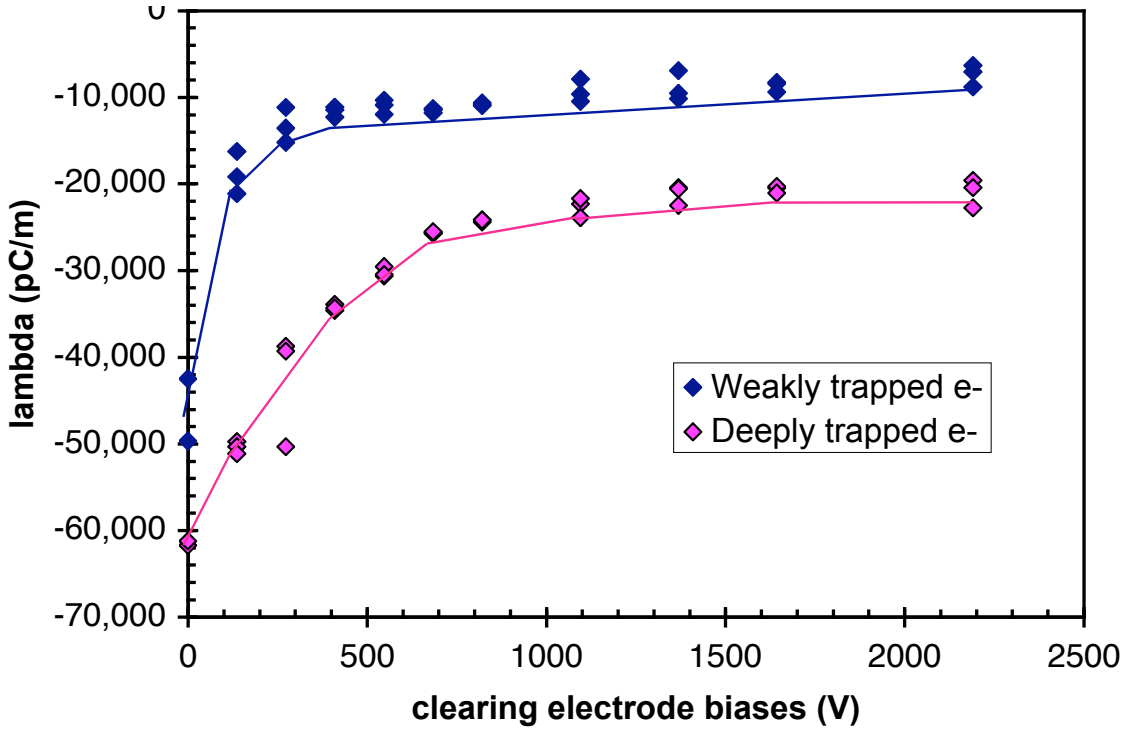

Figure 7. Weakly-trapped electrons (GEC first peak at end of pulse) are removed with lower clearing electrode bias than are deeply-trapped electrons (GEC final peak at end of pulse).

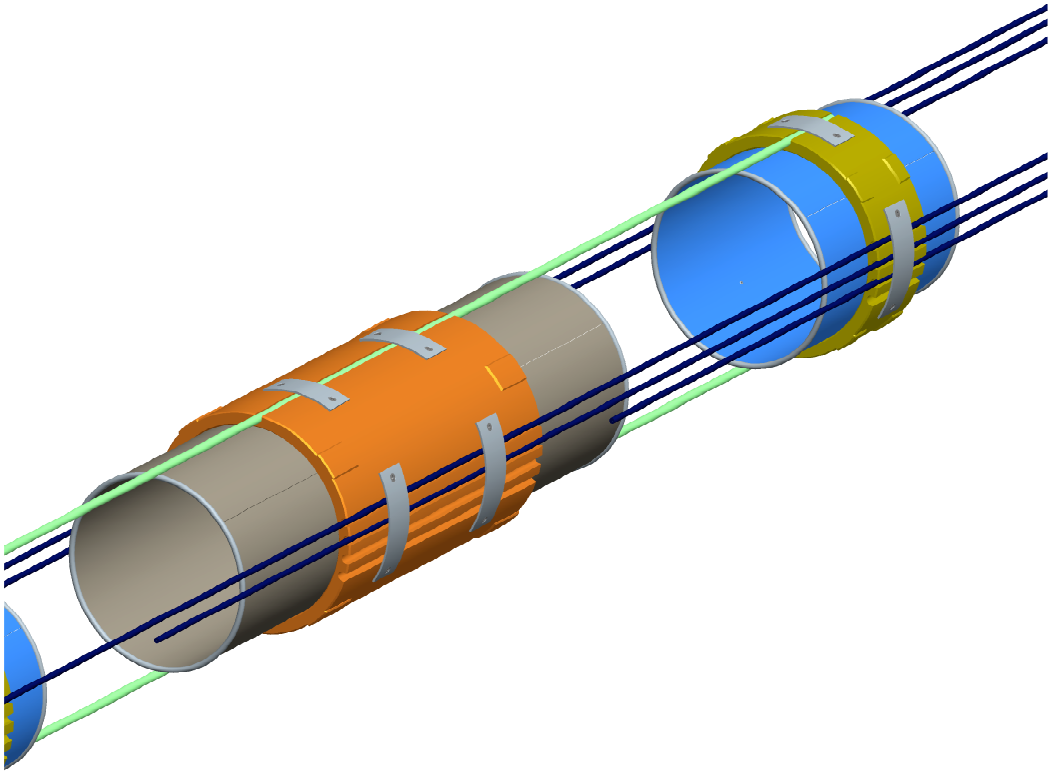

Figure 8. Short biased rings at center of each solenoid magnet and long rings between solenoid magnets are designed to expel or to trap electrons on outer flux lines that intercept the rings between magnets. Only one of each is shown here, four short and three long rings are built for the four solenoids of the STX.

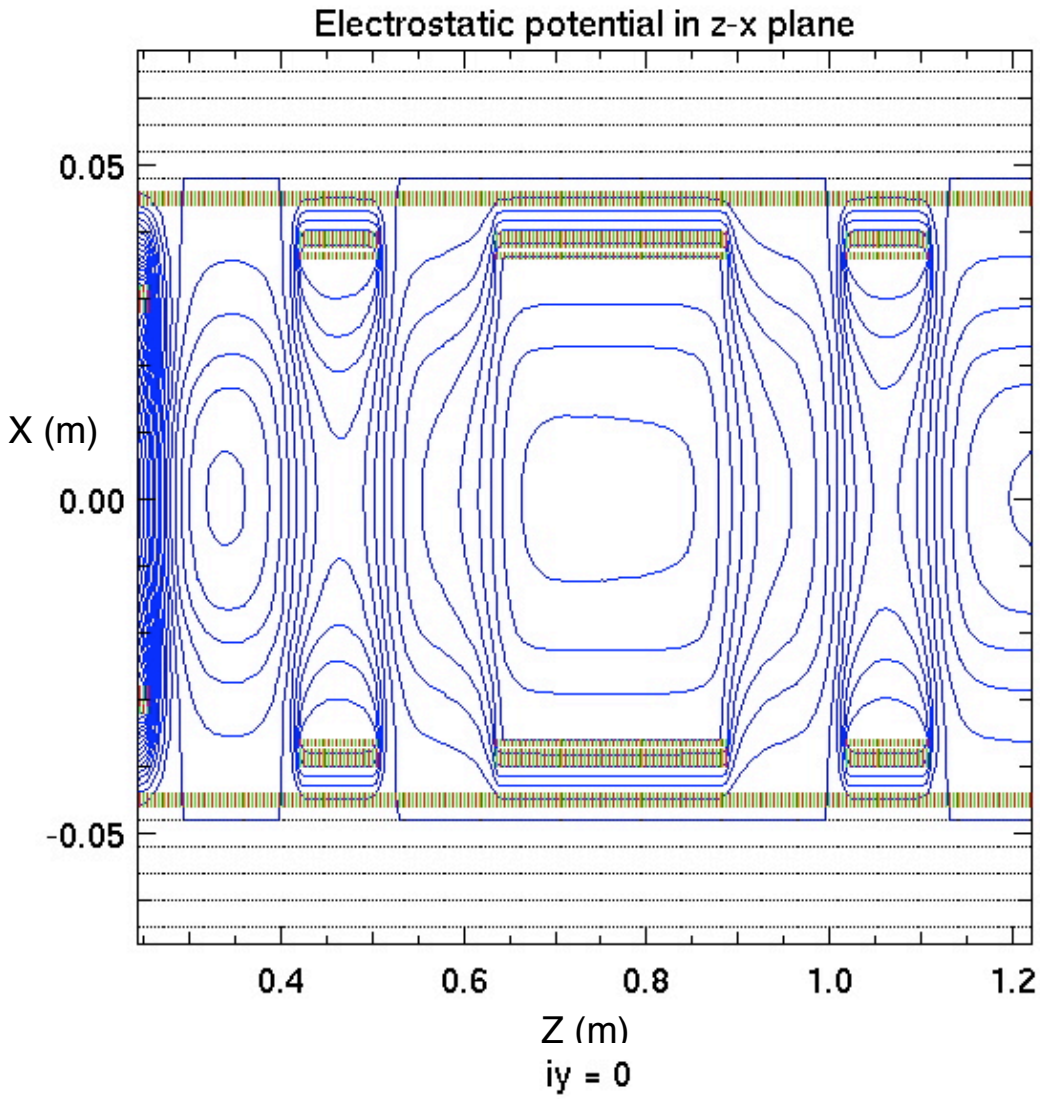

Figure 9. Equipotential contours around short ring at center of solenoid magnet.